DOI: 10.1002/anie.200702466

Metal-Free Catalysis

Nanocarbon as Robust Catalyst: Mechanistic Insight into Carbon-Mediated Catalysis**

Jian Zhang, Dangsheng Su, Aihua Zhang, Di Wang, Robert Schlögl, and Cécile Hébert*

Dedicated to Süd-Chemie on the occasion of its 150th anniversary

Metal-free nanostructured elemental carbons and carbon-based composites (e.g. C_3N_4) have proven to be attractive alternatives to conventional metal-based catalysts for several important reactions, such as dehydrogenation of aromatic hydrocarbons or alkanes, Friedel–Crafts Reaction.[1] Carbon as the catalytic substance has significant advantages over the conventional metal-supported systems owing to the unique controllability of both its surface acidity/basicity and π-electron density through surface functionalization. In a carbon material it is the short- and long-range ordering of atomic carbon that essentially determines the macroscopic properties (e.g. thermal and electronic conductivities, combustibility) and thus its long-term performance in any potential industrial process. However, the lack of basic knowledge on the nature of carbon-mediated reactions remains the most critical restriction for the development of carbon-based catalysis.

For oxidative dehydrogenation (ODH) reactions, surface quinone-type oxygen functional groups have been proposed as the active sites and the reaction has been assumed to proceed by a redox mechanism.[2,3] However, no quantitative description of the elementary steps, or kinetic data can be derived from the literature. The few mechanistic studies reported were conducted either with remarkable secondary oxidation and deactivation[4] or over "impure" surfaces, for example, Pd- or Fe-coordinated polynaphthoquinone[2] or pre-coked metal phosphates or oxides.[5] More detailed and reliable information is expected to be obtained over a pure carbon surface in the kinetic reaction region. Most importantly, the Mars–van Krevelen model for redox reactions is widely accepted based on previous work on the ODH of ethylbenzene.[4,5] However, this model is incorrect and without physical relevance.[6] Therefore there is an urgent need to describe the reaction pathway by a physically relevant model. Ordered nanocarbon is chemically homogeneous and thus could be seen as the most suitable platform for a mechanistic investigation.

To date, all such investigations have been confined to pure or mostly sp^2-hybridized carbons.[4,7] In particular, conventional activated carbon which has long-range disorder and high porosity has been thoroughly studied and claimed to be the efficient catalyst for ODH reaction.[4] Nanodiamond is an sp^3-hybridized carbon and carbon nanotubes are an intermediate state between sp^2-and sp^3-hybridization. Each different hybridization produces a distinct electronic structure for the surface carbon atoms and completely different bulk properties. Moreover, carbon nanotubes are catalytically active but there are no reports on the structure–activity relationships, for example, the effects of tube length, diameter, or thickness.

We report herein, a novel mechanistic understanding of the carbon-mediated ODH of ethylbenzene, in which activated carbon, nanodiamond, and carbon nanotubes with various geometric parameters were tested. We found that the order in the microstructure of the carbon material essentially determines its long-time performance and only nanocarbon could robustly catalyze the ODH reaction. In addition, our model is supported by isotope tracer work.

Intrinsic reaction rates are measured over four commercial nanocarbons: 1) nanodiamond (3–6 nm); 2) nanotube-1: long (3–14 μm) and thick-wall (15 ± 10 walls); 3) nanotube-2: long (1–10 μm) and thin-wall (8 ± 4 walls); and 4) nanotube-3: short (0.1–1 μm) and thin-wall (7 ± 3 walls). Several experiments were carried out separately by varying catalyst pellet size while changing the catalyst loading and flow rates to achieve different liquid hourly space velocity (LHSV). As shown in Figure 1a, the ODH rates over nanotube-1 approach the same value when the LHSV is higher than $8\ h^{-1}$, indicating the absence of mass and heat diffusion artifacts.

Figures 1b and 1c show the performance of all the tested carbons with time on stream at 723 K. For nanocarbons, major byproduct is CO_2 and the concentrations of ethylbenzene, styrene, and CO_2 contribute a closed carbon balance of $100 \pm 2\%$. After a short induction period, each nanocarbon stably catalyzes styrene formation over 1500 minutes. The steady-state styrene selectivity obtained is as high as 95% which indicates success in depressing secondary oxidation. Only the ordered nanocarbon materials perform outstandingly during

[*] Dr. J. Zhang, Dr. D. S. Su, Dr. A.H. Zhang, Dr. D. Wang, Prof. R. Schlögl
Fritz-Haber-Institut der Max-Planck-Gesellschaft
Faradayweg 4–6, 14195 Berlin (Germany)
Fax: (+49) 30-8413-4401
E-mail: dangsheng@fhi-berlin.mpg.de
Dr. C. Hébert
Institut für Festkörperphysik
Technische Universität Wien
Wiedner Hauptstrasse 8–10/138, 1040 Wien (Austria)

[**] This study was supported by European Union as part of the CANAPE and EnerChem projects. The ELNES part was financially supported by USTEM. The authors thank Dr. J. Carlsson for helpful discussion and J. Kröhnert, U. Wild, J. Mizera, and Dr. J. Delgado for assistance with experiments.

Supporting information for this article is available on the WWW under http://www.angewandte.org or from the author.

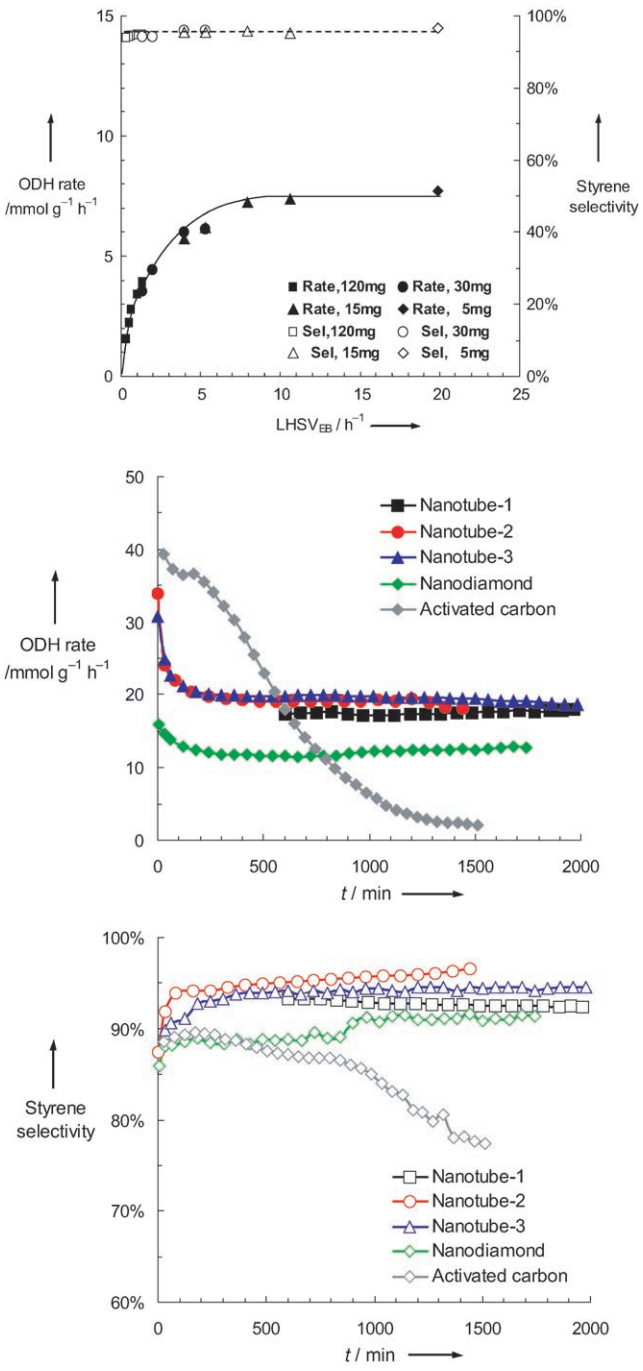

Figure 1. a) ODH reaction rate (mmol g^{-1} h^{-1}) versus LHSV (h^{-1}) (2.8 kPa EB, 1.4 kPa O_2, 95.8 kPa He, 673 K), and styrene selectivity (Sel) over different loadings of nanotube-1. Time dependencies of b) reaction rate and c) styrene selectivity (%) for the ODH of ethylbenzene over nanocarbons in a differential reactor (2.8 kPa EB, 1.4 kPa O_2, 95.8 kPa He, 5 mg catalyst, total SV = 150000 mL g^{-1} h^{-1}, LHSV$_{EB}$ = 20 h^{-1}, 723 K). Commercial activated carbon was tested for comparison. EB = ethylbenzene.

the long-time stability test. One representative commercial activated carbon that has been the subject of previous studies[4] was also evaluated in this work for comparison. The performance of activated carbon differs drastically with those of nanocarbons. As shown in Figures 1b and 1c, a severe deactivation of activated carbon could be clearly detected. After 1600 minutes, the ODH rate was only 5% of the initial one and the selectivity was as low as 76%. Both the carbon balance (over 100%) and high CO_2 yield revealed the deactivation of activated carbon arose from combustion.

Using nanocarbon for styrene synthesis has advantages over the multi-promoted iron catalysts used in the direct dehydrogenation processes. By introducing small amount of O_2 (O_2/ethylbenzene = 0.5), nanocarbon is comparable to or even more active and selective than the typical iron catalysts, even at the temperature for around 200 K lower (Supporting Information, Table S1). Note that we did not introduce any steam in the for ODH tests. However, for the commercial direct dehydrogenation (DH) process, steam (with the high steam/oil ratio (S/O)) is always required to provide heat for the endothermic reaction and to regenerate the iron-based active site from coking, which results in large energy consumption.

The structural and electronic properties of nanotubes and nanodiamond are quite different, which should influence the electron-transport rate inside the carbon matrix and thus their catalytic behavior. Measurements of reaction orders and activation energies provide insight into the mechanism of the reaction. No convincing kinetic parameters could be obtained over the very unstable activated carbon. Over each nanocarbon, we derived the reaction orders for ethylbenzene or O_2 from the linear $\ln R \approx \ln P_i$ relationship (Supporting Information, Figure S1) and the Arrhenius activation energy from the ODH reaction rates at different temperature (Supporting Information, Figure S2), in which the related regressive coefficient is always higher than 0.99. The derived kinetic parameters are listed in Table 1. Surprisingly, the reaction orders with respect to O_2 and ethylbenzene and activation energies over all the tested nanocarbons are around 0.32 ± 0.05, 0.56 ± 0.10, and 73 ± 5 kJ mol^{-1}, respectively. Especially after normalizing the overall rate by specific surface area, the sp^3-nanodiamond and predominantly sp^2-nanotubes are similarly active, that is, the rate at 723 K and pre-exponential factor are around 4.7×10^{-2} mmol m^{-2} h^{-1} and $(5.4 \pm 0.5) \times 10^3$ mmol m^{-2} h^{-1} kPa^{-1}, respectively. Strict correlation between reaction kinetics and mechanism allows us to confirm that the same reaction pathway involving the same active sites occurs in the various nanocarbons employed. This result is contrary to the fact that the structural and electronic properties of nanotube and nanodiamond are quite different, which is expected to influence the electron-transport rate inside carbon matrix and thus their catalytic behavior. Analysis of the reason is detailed together with characterization results, see below.

We fitted the measured kinetic data by each possible reaction model for the ODH of hydrocarbon molecules (Langmuir–Hinshelwood, Eley–Rideal, or surface oxido reduction).[6] During the calculation, the objective function was the minimization of the sum of squares of the difference between the measured and calculated value for the extent of reaction. As shown in the Supporting Information, Figure S3, the kinetic data agreed well with the dual-site Langmuir–Hinshelwood model including dissociative adsorption of oxygen molecules and noncompetitive adsorption between

Table 1: Kinetic parameters for ODH of ethylbenzene over nanocarbons (573–723 K).[a]

Nanocarbon	ODH rate at 723 K		Activation energy	Pre-exponential factor, k_o		Reaction order	
	[mmol $g^{-1} h^{-1}$]	[mmol $m^{-2} h^{-1}$][b]	[kJ mol^{-1}]	[mmol $g^{-1} h^{-1} kPa^{-1}$]	[mmol $m^{-2} h^{-1} kPa^{-1}$][b]	Ethylbenzene	O_2
Nanotube-1	16	4.6×10^{-2}	75	$(2.0\pm0.2)\times10^{6}$	$(5.3\pm0.5)\times10^{3}$	0.51 ± 0.05	0.30 ± 0.03
Nanotube-2	19	–	71	$(1.4\pm0.1)\times10^{6}$	–	0.52 ± 0.06	0.34 ± 0.04
Nanotube-3	20	–	68	$(0.9\pm0.1)\times10^{6}$	–	0.55 ± 0.04	0.32 ± 0.03
Nanodiamond	12	4.9×10^{-2}	75	$(1.4\pm0.2)\times10^{6}$	$(5.5\pm0.6)\times10^{3}$	0.61 ± 0.10	0.33 ± 0.07

[a] Reaction conditions: 5 mg catalyst, 2.8–6.4 kPa ethylbenzene, 1.4–8.4 kPa O_2, He as balance. [b] Normalized by specific surface area of used sample in steady state.

ethylbenzene and oxygen molecules. In this mechanism, the overall reaction rate is kinetically limited by the rate of the surface reaction, which mainly involves breaking of two C–H bonds in ethylbenzene at the α and β positions.

The model proposed is corroborated by isotopic tracer studies carried out by replacing the hydrocarbon by its deuterium-labeled analogue, a technique which is widely used to reveal whether or not a particular bond is directly involved in the rate-limiting step.[8] As shown in Figure 2, after switching the reactant mixture from $C_6H_5C_2H_5/O_2$/He to $C_6D_5C_2D_5/O_2$/He, the reaction rate decreased from 16.7 to 11.9 mmol $g^{-1} h^{-1}$ over Nanotube-1 at 723 K. This

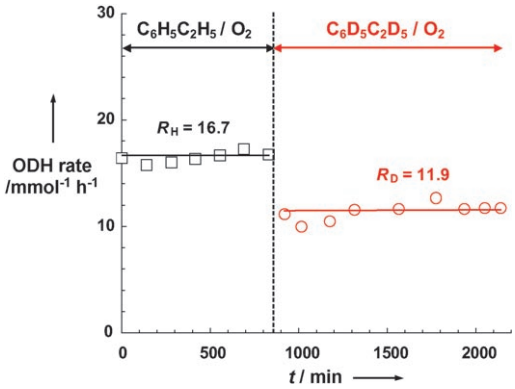

Figure 2. Reaction rate (mmol $g^{-1} h^{-1}$) with $C_6H_5C_2H_5/O_2$ and $C_6D_5C_2D_5/O_2$ reaction mixtures on nanotube-1 (2.8 kPa EB, 1.4 kPa O_2, He as balance, 5 mg catalyst, $LHSV_{EB} = 20\ h^{-1}$, 723 K).

result demonstrates a clear kinetic isotopic effect ($R_H/R_D = 1.4$) and confirmed the relevance of C–H bond activation in the reaction mechanism.

To identify the active phase and the reason for the similar kinetics found over all the nanocarbons, we performed microscopic and spectroscopic characterizations of fresh and used samples. The long-time stability of nanocarbon, which is superior to that of activated carbon, is explained by its robust microstructure. As shown in Figure 3, after a long-time ODH reaction, the tubular graphite or the nanodiamond structure is fully intact and no evidence of combustion could be

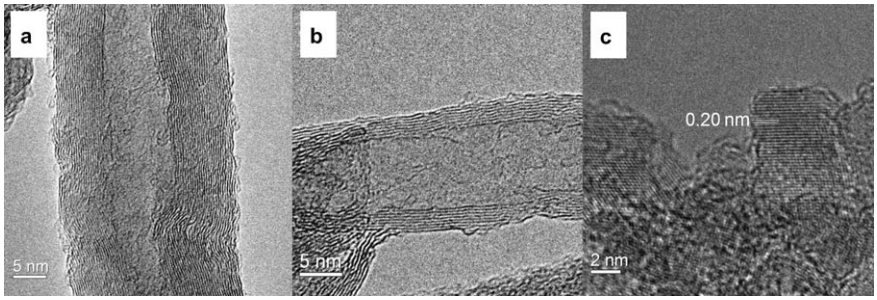

Figure 3. HRTEM images of used nanocarbons: a) nanotube-1; b) nanotube-2; c) nanodiamond.

detected.[9] Most importantly, the used nanotubes and nanodiamond are clean and free of observable coking or deposited carbon. Temperature-programmed oxidation (TPO) spectra of used nanocarbons showed no low-temperature peak corresponding to polymer-like coking, in agreement with the microscopy evidence. Quantification of ex-situ X-ray photoelectron spectra revealed a slight decrease (±4–7%) of the surface O/C ratio after reaction, suggesting a surface reconstruction process to form stable active sites and that the deactivation in the initial stage of catalysis might arise from removal of unstable active groups.[10] For nanodiamond, the loss in activity is lower than for nanotubes (Figure 1b), which might be explained by the compensation gained from generating more stable sites by a slight surface transformation of nanodiamond into a functionalized single or double atomic layer under oxidative environment. Evidence for this transformation is shown in Figure 3c, in which the edge of the used nanodiamond seems different to the sp^3-carbon in bulk.

Such reconstruction process could also be identified by quantification of the electron energy-loss near edge structure (ELNES) spectra of carbon K-edge of nanotubes and nanodiamonds before and after reaction (Figure 4). The ELNES of highly orientated pyrolitic graphite (HOPG) sample was included as reference for quantification of the sp^2/sp^3 ratio. Two spectral features centered at approximately 285 eV and approximately 292 eV indicate π* and σ* transitions, the latter is typical for graphite or sp^2-bond carbon.[9] After the ODH reaction for 1800 minutes, the specific fine structure for the nanotube and nanodiamond remained. Quantitative analysis indicates that the fraction of sp^2-carbon in the nanotube decreased from 80±3% to 75±5% while that of sp^3-carbon in nanodiamond decreased from 93±1% to 87±3%, indicating that the stable active sites that survived or formed during the initial stage of the ODH reaction are

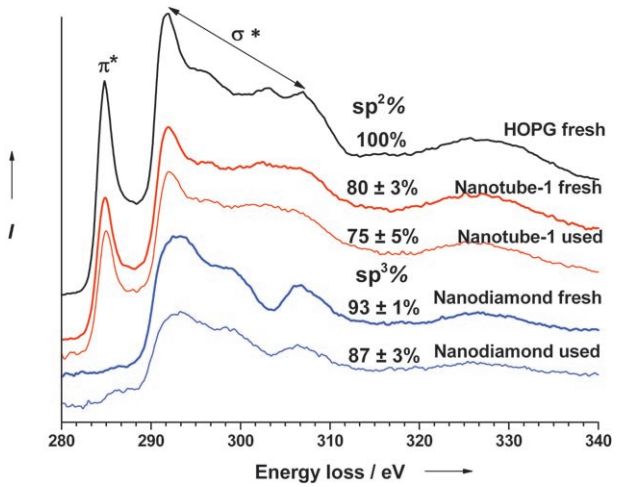

Figure 4. ELNES spectra of fresh and used nanocarbons.

defective and comprise both sp^2- and sp^3-hybridized carbons. From this viewpoint, the subsurface structure of nanocarbon did not influence its activity in the ODH reaction, a feature not found for the metal-based catalysts.

IR spectroscopy gave clear spectra of nanodiamond before and after reaction (Supporting Information, Figure S4). A strong band at 1790 cm^{-1} arose from the stretching C=O vibration in quinine or carbonyl groups.[10,11] After reaction, this band remained but slightly shifted to 1750 cm^{-1}. This evidence is in agreement with the previous studies on onionlike carbon, in which surface carbonyl was demonstrated to be the most active phase by quasi in-situ X-ray photoelectron spectroscopy (XPS) studies.[12] No bands at 3020 and 3080 cm^{-1}, corresponding to vibrations of C–H aromatic, could be observed, in agreement with the absence of amorphous carbon in the TEM images.[2,5]

Important characteristic information from this study is that: 1) the robust catalytic performance of nanocarbons arises from almost unchanged morphologies and bulk structure and the absence of coking and/or combustion over a long reaction time (TEM/TPO/IR); 2) the survival of or formation of stable active sites leads to a deactivation at the beginning of the reaction (IR/XPS); and, 3) both sp^2-nanotube and sp^3-nanodiamond have similar active sites comprising both sp^2- and sp^3-hybridized carbon atoms, a feature which could explain their similar kinetics (ELNES).

To summarize, we report a novel mechanistic study on nanostructured carbons as the catalysts for oxidative dehydrogenation of ethylbenzene. The robust and outstanding activity of nanocarbon indicates a great potential for its use in the styrene industry. The reaction obeys the dual-site Langmuir–Hinshelwood mechanism, in which the breaking of C–H bonds is kinetically relevant. The reaction pathway and nature of the active sites are shown to be same over both sp^2-nanotube and sp^3-nanodiamond. The π-conjugation effect of the graphite structure does not seem to be essential for nanocarbon to function as a catalyst. Our mechanistic findings differ in from those for the metal or metal oxide catalysts involving lattice oxygen that have been seen as one of the most active phases.

Experimental Section

Thick-walled carbon nanotubes (nanotube-1) was provided by Tsinghua University (China) while thin-walled carbon nanotubes with different length (nanotube-2 and nanotube-3) were bought from Nanocyl (Belgium). Parameters (length, outer diameter, wall number) of such three samples are: nanotube-1 (3–14 μm, 25 ± 10 nm, 15 ± 10), nanotube-2 (1–10 μm, 11 ± 4 nm, 8 ± 4), and nanotube-3 (0.1–1 μm, 10 ± 3 nm, 7 ± 3). All of these samples were pretreated by refluxing in concentrated HNO_3 (54%) for 2 h and then immersing in the mother liquor at room temperature overnight to remove the metal impurities. Nanodiamond with average size 5 nm (Beijing Institute of Technology) was prepared by the detonation explosive method followed by acid washing. TPO/TG tests revealed the contents of ash residuals in such four nanocarbons are 3.8%, 0.6%, ca. 0.0%, and 2.0%, which are mainly inert oxides. Acid-washed activated carbon (ROX 0.8, 950 $m^2 g^{-1}$) was produced by Norit Deutschland GmbH.

Kinetic selectivity and rate measurements were carried out in a fixed-bed quartz reactor using catalyst (5 mg) without mass transfer artifact. SiC pellets (500 mg; Aldrich–Sigma) was added to prevent temperature gradients. The reactant consisted of ethylbenzene and O_2 at 2.8 and 1.4 kPa, respectively. Helium was used as the diluent to maintain the reaction at an atmospheric pressure. Typical total gas flow rate was 12.5 mL min^{-1} while the liquid hourly space velocity of ethylbenzene was 20 h^{-1}. Online analysis of reactants and products was performed on a Varian CP-3800 gas chromatograph equipped with TCD and FID detector. Typical ethylbenzene and O_2 conversions were less than 20%. Blank experiments using pure SiC or empty reactor showed that reaction rates were negligible without nanocarbon. Rates are reported as mmol of styrene produced per gram of nanocarbon per hour (mmol $g^{-1} h^{-1}$).

SEM micrographs were taken on a Hitachi S-4800 at an acceleration voltage of 3 kV. TEM micrographs and ELNES spectra were obtained from a Phillips CM200-FEG and a TECNAI F20-FEG at an acceleration voltage of 200 kV. The ELNES were recorded under magic angle conditions taking into account the relativistic correction to avoid effects of anisotropy.[13] The sp^2/sp^3 ratio was obtained by fitting the first part of the C-K ELNES with 3 Gaussians centered at around 285, 287, and 292 eV following the procedure proposed by Ref. [14]. Thermal gravimetry (TG) analysis was performed by using a Netzsch STA-449C microbalance with a heating rate of 5 K min^{-1} in a flow of 20% O_2/He. Transmission IR spectra were recorded on a Perkin–Elmer 2000 FTIR. XPS characterization was performed using a VG RSCA LABMK II spectrometer equipped with $Al_{K\alpha}$ radiation.

Received: June 6, 2007
Published online: August 23, 2007

Keywords: heterogeneous catalysis · nanocarbon · oxidative dehydrogenation · reaction mechanisms · styrene

[1] a) N. Keller, N. I. Maksimova, V. V. Roddatis, M. Schur, G. Mestl, Y. V. Butenko, V. L. Kuznetsov, R. Schlögl, *Angew. Chem.* **2002**, *114*, 1962–1966; *Angew. Chem. Int. Ed.* **2002**, *41*, 1885–1888; b) F. Goettmann, A. Fischer, M. Antonietti, A. Thomas, *Angew. Chem.* **2006**, *118*, 4579–4583; *Angew. Chem. Int. Ed.* **2006**, *45*, 4467–4471; c) Z.-J. Sui, J.-H. Zhou, Y.-C. Dai, W.-K. Yuan, *Catal. Today* **2005**, *106*, 90–94; d) J. de J. D. Velásquez, L. M. C. Suárez, J. L. Figueiredo, *Appl. Catal. A* **2006**, *311*, 51–57; e) I. F. Silva, J. Vital, A. M. Ramos, H. Valente, A. M. B. Rego, M. J. Reis, *Carbon* **1998**, *36*, 1159–1165.

[2] Y. Iwasawa, H. Nobe, S. Ogasawara, *J. Catal.* **1973**, *31*, 444–449.

[3] G. Mestl, N. I. Maksimova, N. Keller, V. V. Roddatis, R. Schlögl, *Angew. Chem.* **2001**, *113*, 2122 – 2125; *Angew. Chem. Int. Ed.* **2001**, *40*, 2066 – 2068.
[4] a) M. F. R. Pereira, J. J. M. Órfão, J. L. Figueiredo, *Appl. Catal. A* **2000**, *196*, 43 – 54; b) M. F. R. Pereira, J. J. M. Órfão, J. L. Figueiredo, *Appl. Catal. A* **2001**, *218*, 307 – 318.
[5] a) G. Emig, H. Hofmann, *J. Catal.* **1983**, *84*, 15 – 26; b) A. Schraut, G. Emig, H. Hofmann, *J. Catal.* **1988**, *112*, 221 – 228.
[6] a) M. A. Vannice, *Catal. Today* **2007**, *123*, 18 – 22; b) M. M. Barsan, F. C. Thyrion, *Catal. Today* **2003**, *81*, 159 – 170.
[7] a) D. S. Su, N. Maksimova, J. J. Delgado, N. Keller, G. Mestl, M. J. Ledoux, R. Schlögl, *Catal. Today* **2005**, *102–103*, 110 – 114; b) J. J. Delgado, D. S. Su, G. Rebmann, N. Keller, A. Gajovic, R. Schlögl, *J. Catal.* **2006**, *244*, 126 – 129; c) P. Li, T. Li, J.-H. Zhou, Z.-J. Sui, Y.-C. Dai, W.-K. Yuan, D. Chen, *Microporous Mesoporous Mater.* **2006**, *95*, 1 – 7.
[8] a) K. J. Laidler, *Chemical Kinetics*, 3rd ed., Harper & Row publisher, **1987**; b) J. M. Wei, E. Iglesia, *Angew. Chem.* **2004**, *116*, 3771 – 3774; *Angew. Chem. Int. Ed.* **2004**, *43*, 3685 – 3688.
[9] a) S. Osswald, G. Yushin, V. Mochalin, S. O. Kucheyev, Y. Gogotsi, *J. Am. Chem. Soc.* **2006**, *128*, 11635 – 11642; b) V. V. Roddatis, V. L. Kuznetsov, Yu. V. Butenko, D. S. Su, R. Schlögl, *Phys. Chem. Chem. Phys.* **2002**, *4*, 1964 – 1967.
[10] a) J.-H. Zhou, Z.-J. Sui, J. Zhu, P. Li, D. Chen, Y.-C. Dai, W.-K. Yuan, *Carbon* **2007**, *9*, 1379 – 1389; b) J. L. Figueiredo, M. F. R. Pereira, M. M. A. Freitas, J. J. M. Órfão, *Carbon* **1999**, *37*, 1379 – 1389.
[11] a) E. Mironov, A. Koretz, E. Petrov, *Diamond Relat. Mater.* **2002**, *11*, 872 – 876; b) B. V. Spitsyn, J. L. Davidson, M. N. Gradoboev, T. B. Galushko, N. V. Serebryakova, T. A. Karpukhina, I. I. Kulakova, N. N. Melnik, *Diamond Relat. Mater.* **2006**, *15*, 296 – 299; c) A. Dandekar, R. T. K. Baker, M. A. Vannice, *Carbon* **1998**, *36*, 1821 – 1831.
[12] J. A. Maciá-Agulló, D. Cazorla-Amorós, A. Linares-Solano, U. Wild, D. S. Su, R. Schlögl, *Catal. Today* **2005**, *102–103*, 248 – 253.
[13] C. Hébert, P. Schattschneider, H. Franco, B. Jouffrey, *Ultramicroscopy* **2006**, *106*, 1139 – 1143.
[14] A. C. Ferrari1, A. Libassi, B. K. Tanner, V. Stolojan, J. Yuan, L. M. Brown, S. E. Rodil1, B. Kleinsorge, and J. Robertson, *Phys. Rev. B* **2000**, *62*, 11089 – 11103; S. D. Berger, D. R. McKenzie, P. J. Martin, *Philos. Mag. Lett.* **1988**, *57*, 285 – 290.

